Investigation of residual strain in quartzite using neutron diffraction: interpretation and self-consistent modelling

Jean-Claude Guezou, Hiba Azzeddine, Monica Ceretti, Thierry Baudin

Investigation of residual strain in quartzite using neutron diffraction: interpretation and self-consistent modelling

Jean-Claude Guezou[1], Hiba Azzeddine[2,*], Monica Ceretti[3], Thierry Baudin[4]

[1] Sciences de la Terre, UMR CNRS 7072, Université de Cergy-Pontoise, France.

[2] Laboratoire Matériaux et Energies renouvelables, Faculté des Sciences, Université Mohamed Boudiaf, M'sila, 28000, Algérie.

[3] ICGM, Univ. Montpellier, CNRS, ENSCM, Montpellier, France

[4] Université Paris-Saclay, CNRS, Institut de chimie moléculaire et des matériaux d'Orsay, 91405 Orsay, France.

* Corresponding author: Pr. Hiba Azzeddine, hiba.azzeddine@univ-msila.dz

Abstract

The residual strain determination by neutron diffraction has been performed on a set of five natural quartzite samples collected from Betic Cordilleras (Spain) and Sivas Basin (Turkey). The starting idea was to document an earlier conclusion about the texture components related either to deformation or recrystallization phenomena. Thereafter, as a consequence of the rock inhomogeneity, the complete strain tensor has been determined for each sample and discussed by taking into consideration the present-day knowledge in material sciences. The imposed macroscopic deformation observed at the sample locality led us to consider the form of the residual strain tensor as possibly representative of the natural finite plastic deformation suffered at the sample scale. Based on this, those tensors have been fitted to plastic tensors and introduced in texture simulations using a visco-plastic self-consistent (VPSC) model. The results demonstrate that the complete and meaningful strain tensor determination in rocks could be used as an experimental input in numerical modeling. This new combination of experimental and numerical approaches was validated and could help to better understand some geological phenomena.

Keywords: Quartzite; Neutron diffraction; Residual elastic strain; Strain tensor; Texture; VPSC modelling.

1. INTRODUCTION

Quartz is one of the well-known and well-studied mineral phases. Deformed quartz-rich rocks like sandstone and quartzite are rather ubiquitous in upper crustal faults and mountain belts taking place in the upper part of the earth's crust. The microstructure and the crystallographic texture (also referred by geologists as 'fabric' or 'crystallographic preferred orientation') of quartzite were first used to characterize the deformation behaviour in rocks and to evaluate their kinematics (Sander 1950). Following the removal of stresses, residual strains are often trapped by defects within crystal lattices. It is expected that this process is strongly controlled by the texture evolution (Frischbutter et al. 2006). Usually, the microstructures and crystallographic textures are interpreted empirically in connection with the macroscopic and regional strain derived from geological studies owing to the difficulties in conducting reliable direct experiments at extreme conditions such as high temperature and pressure (Schmid 1994). Through links with materials science, both theoretical aspects and numerical modelling of texture developments have been put forward in a series of publications (Kocks, Wenk and Tomé 2000). Most of these advancements have been concerned with the grain crystallographic orientation distribution and behaviour in very common and nearly single phase polycrystalline geomaterials such as quartzite, marble, peridotite under natural deformation.

A physical approach of texture development of quartzite polycrystals has been first tested by means of the current Taylor model (Lister and Hobbs 1980). Much closer predictions of these textures have been obtained with the Visco-Plastic Self Consistent (VPSC) model (Wenk et al. 1989, Takeshita, Wenk and Lebensohn 1999, Guezou et al. 2001, Morales, Lloyd and Mainprice 2014, Wenk et al. 2019). Nevertheless, a simulation giving way to a closer representation of the real textures still needs a complete knowledge about textures and microstructural/micromechanical information completed by laboratory experiments.

A previous study was attempted to correlate the main types of microstructures documented in quartzite with the corresponding crystallographic texture (Albertini et al. 1991). This correlation is obviously very difficult as the natural quartzite samples often present a combination of deformed and statically and/or dynamically recrystallized grains in the observed microstructure. However, schematically, the authors have identified two different deformation and recrystallization microstructures and textures. Such as in metals, according to markers of the deformation history (grain boundary aspect, grain substructure, grain size, grain shape, …), the microstructural observations have shown that the most

deformed samples were mainly sheared, leading to elongated grains in the foliation plane. These grains possess classically a subgrain structure. On the contrary, some other samples were entirely recrystallized and present equiaxed grains free of dislocations. The grain size is thus related to the type of recrystallization but also to the possible grain growth phenomenon after recrystallization. Concerning the crystallographic aspect, it was found that the deformed quartzite samples exhibit a strong texture with the formation of the $\{\bar{1}2\bar{1}0\}<\bar{1}010>$ component while the recrystallized ones were characterized by a weak texture with the presence of the $\{\bar{1}10\bar{1}\}<\bar{1}\bar{1}20>$ component. Figure 1 presents the ideal position of $\{\bar{1}2\bar{1}0\}<\bar{1}010>$ and $\{\bar{1}10\bar{1}\}<\bar{1}\bar{1}20>$ orientations in the {0001} pole figure firstly found in quartzites selected within a well-defined geological area (Albertini et al. 1991). On one hand, the deformation component is defined by a single maximum located in the pole figure centre, i.e. along the transverse direction of the foliation plane and then, perpendicular to the lineation direction (Figure 1a). On the other hand, Figure 1b shows that the recrystallization component is characterized by two maxima rotated around the lineation direction and located at 40-50° from the pole figure centre (Albertini et al. 1991).

Neutron diffraction is one of the most powerful techniques for texture characterization and for measuring residual strain of rock materials (Hutchings and Krawitz 1992, Brokmeier 1994, Guezou et al. 1999, Walther, Scheffzük and Frischbutter 2000, Scheffzük, Walther and Frischbutter 2001, Tanaka, Akiniwa and Hayashi 2002, Hunter, Luzin and Wilson 2017, Wenk et al. 2019, Zucali, Chateigner and Ouladdiaf 2020). Some significant advantages of the neutron diffraction for strain analysis in rocks are the absence of absorption which permits a deep penetration inside the rocks, where small volumes of grains are preserved from a complete relaxation by mechanical treatments during the sampling. The heterogeneous distribution of the grain size observed in the natural rocks has no effect on the accuracy of the texture measurements since large volume fraction of grains can be investigated. Moreover, complete pole figures can be obtained in transmission and the {0001} pole figures commonly discussed in the geological literature are significantly sharper. The roughness of the surface of the sample can be neglected hence the mechanical preparation by grinding and polishing of the sample surface is not necessary. The latter point is particularly convenient for successively handling the sample in a series of non-destructive tests.

The aim of the present experimental investigation is to evaluate the residual stress tensor by neutron diffraction according to the nature of texture evolution (deformation and recrystallization textures). In addition, the effect of experimental conditions, such as diffracting gauge volume and measuring position at the sample, on the residual strain

evaluation were investigated. Finally, the experimental calculated residual strain tensors were used as input data for texture modelling through VPSC model. Therefore, this study allows to validate this original combination of experimental and numerical approaches and to estimate its limitations before using it to understand the geological features, such as for example the chronology of tectono-metamorphic events.

2. Residual strain analysis

Before going further, it is helpful to present some basics of residual strain/stress measurement/calculation by neutron diffraction.

2.1. Residual strain/stress basics

The neutron diffraction technique for strain analysis came up during the eighties and it is now widely used in material sciences for strain/stress measurements/calculations (Hutchings and Krawitz 1992). Currently, the determination of the residual elastic strain tensor using neutron diffraction is largely used for the geomaterials (Guezou et al. 1999, Frischbutter et al. 2000, Guezou et al. 2001, Frischbutter et al. 2006, Scheffzük, Siegesmund and Koch 2004, Wenk et al. 2020).

The theory of residual stress evaluation has been described in several review papers (Dölle 1979, Noyan and Cohen 1987, Withers and Bhadeshia 2001). Basically, the residual stresses originate from three basic physical sources: the plastic flow, thermal contraction and volume change. The total residual stress state in a point of the material is determined by the superposition of the three kinds of stresses named σ^{I}, σ^{II} and σ^{III}. A schematic illustration of the three orders of residual stresses is shown in Figure 2 and they have been conventionally defined as follows (Macherauch and Kloos 1986):

- Residual stresses of the first order (σ^{I}), named also type I stresses, are nearly homogeneous across large areas, in the order of several grains of the material (at a scale about 10^{-1} mm) and are equilibrated within the whole body. The magnitude corresponds to a mean value over the volume of grain involved within the gauge volume (Figure 2). Thus, type I stresses by definition are independent of the orientation of individual grains. These stresses are also called macro residual stresses.
- Residual stresses of the second order (σ^{II}), named type II stresses, are nearly homogeneous across microscopic areas, of the order of a single grain or a phase (about 10^{-3} mm) and are equilibrated across a sufficient number of grains. Type II stresses are grain orientation dependent. This means that for a given stress component, the sign and magnitude of the

type II stress within a grain is dependent on the orientation of the grain with respect to the specimen directions. These stresses are called homogeneous micro residual (mesoscopic) stresses.

- Residual stresses of the third order (σ^{III}), named type III stresses, are inhomogeneous across sub microscopic areas of the material, several atomic distances within a grain (10^{-6} mm), and are equilibrated across small part of a grain. These stresses are the inhomogeneous micro residual stresses.

Practically, it is difficult to distinguish the effects of the second and third order, so the micro stresses are generally defined as the sum of the two latter. All three kinds of stresses can be estimated from experimental measurements.

The second order stresses are usually ascribed to strain incompatibilities along both side of a grain boundary (an illustration of the concept of necessary geometric dislocations). The third order stresses have been related to walls and dislocations cells inside the grain. The two orders are accordingly related to the dislocation patterns delivered from the processes of intergranular accommodation. It is well known that the stored energy calculation is based on the quantification of dislocation density. Hence, the residual micro stresses evaluations can be considered as another method for stored energy measurement and also can be related to the lattice spacing distortion (Haworth 1937).

2.2. Residual elastic strain measurements

To sum up, depending on the forming process and/or thermal treatments of materials, various physico-mechanical phenomena of metallurgical (phase change), thermal (inhomogeneous cooling) or mechanical (anisotropic and heterogeneous strain) origin can occur and generate plastic strain incompatibilities. These last ones are compensated by irreversible elastic strains and are at the origin of internal stresses from a mechanical point of view.

The elastic residual strain determination by diffraction methods implies the measurement of the lattice spacing d under stress. In comparison with the initial interplanar lattice spacing $d_{0,}$ measured on a stress-free reference sample, this strain varies proportionally with Δd_{hkil} (where $hkil$ are the Miller's indices of the considered diffracting plane). According to the Bragg's law, it becomes possible to link a small lattice strain to a shift of the scattering angle ($\Delta 2\theta_{hkil}$) by the following relation:

$$\varepsilon = \left(\frac{d-d_0}{d_0}\right)_{\square kil} = \left(\frac{\Delta d}{d_0}\right)_{\square kil} = -\frac{1}{2}\cot\,\theta_0.\Delta 2\theta_{\square kil} \qquad (1)$$

The strain ε is measured in the direction of the scattering vector $\vec{Q}(\phi\psi)$, the orientation of which is defined conventionally by the angles ϕ and ψ with respect to the sample coordinate system as illustrated in Figure 3. Indeed, the diffraction measures the mean interplanar spacing $(d_{hkil,\varphi,\psi})_{Vd}$, averaged for the diffracting grains (V_d) that have the vector $\vec{Q}(\phi\psi)$ normal to the considered planes. Interesting to recall that the quartzite has a trigonal crystal symmetry. The average strain should be written in a general form with the contributions of the intergranular strains related to the elastic, plastic and thermal components (Gloaguen, François and Guillen 2004).

Then, the strain along the direction $\vec{Q}(\phi\psi)$ is related to the tensor components ${\varepsilon_{(\square kil)}}^{\phi\psi}$ defined in the sample coordinates (LD, TD, ND) and transformed into the general equation:

$$ {\varepsilon_{(\square kil)}}^{\phi\psi} = \varepsilon_{11}\, cos^2\,\phi\, sin^2\,\psi + \varepsilon_{22}\, sin^2\,\phi\, sin^2\,\psi + \varepsilon_{33}\, cos^2\,\psi + \varepsilon_{12}\, sin\,2\,\phi\, sin^2\,\psi + \varepsilon_{13}\, cos\,\phi\, sin\,2\,\psi + \varepsilon_{23}\, sin\,\phi\, sin\,2\,\psi \quad (2) $$

For the determination of the complete strain tensor, measurements of the deformation in different orientations $\vec{Q}(\phi\psi)$ are required to solve the algebraic system with the six components of the strain tensor as unknowns. Practically, the complete strain tensor components are obtained from equation (2) by a multilinear regression based on least square fittings of at least six directions ($\phi\psi$). This technique is known as the conventional $\sin^2\psi$-method often used to determine the residual strain by X-ray and neutron diffraction (Macherauch, Müller and Angew 1961, Ruud 1982, Guo et al. 2021).

The non-trivial problem of the strain calculation is the determination of the strain free references $d_0(hkil)$ of the investigated material. In this case, using a powder which is considered completely relaxed of σ^I and σ^{II} order stresses can be a solution to derive the strain free value $d_0(hkil)$ of the studied material.

3. MATERIALS AND METHODS

3.1 Quartzite samples

The strain measurements were performed on three quartzites samples named: 131, 59 and 14 collected from Betic Cordilleras (Spain) and two other samples named TA and TB collected from Sivas Basin (Turkey).

In the present study, the sample 131 presents the deformed state, samples TB and TA are partially recrystallized and samples 59 and 14 are completely recrystallized.

The deformed 131 sample contains brittle second phase mainly epidote mineral embedded in the quartz matrix as shown in Figure 4.

3.2. Neutron diffraction experiments

Textures were characterized using the 6T1 diffractometer at the L.L.B. (C.E.A., Saclay, France) with a wavelength of 1.158 Å. A set of five complete pole figures ($\{10\bar{1}0\}$, $\{10\bar{1}1\}$, $\{11\bar{2}0\}$, $\{11\bar{2}1\}$ and $\{20\bar{2}1\}$) was measured in transmission mode for each sample. The {0001} pole figure was calculated from the Orientation Distribution Function (ODF) by using 'de la Vallée Poussin' kernel with 5° halfwidth. The recalculated {0001} pole figures are presented in equal area projection and their intensities are expressed in multiple random distribution (mrd).

The degree of texture strength of each sample was calculated based on the following equation (Skrotzki et al. 2010):

$$I = \frac{1}{8\pi^2}\int_G f^2(g).dg \quad (4)$$

Where *I* is texture strength index, *f(g)* is the ODF and *G* is the Euler space.

The volume fraction of the deformation $\{\bar{1}2\bar{1}0\}<\bar{1}010>$ and recrystallization $\{\bar{1}10\bar{1}\}<\bar{1}\bar{1}20>$ components was defined by the ratio of volume element $\Delta V(g)$ corresponding to the orientation *g*, to the volume of the entire ODF, V_{Total} following the equation (Suwas and Ray 2014):

$$V_F(g) = \frac{\Delta V(g)}{V_{Total}} \quad (5)$$

$\Delta V(g)$ is related to the ODF in a given volume *V*, by the following equation (Suwas and Ray 2014):

$$\frac{dV(g)}{V} = f(g)dg \quad (6)$$

The texture data were analysed by the free MTEX toolbox for Matlab (Bachmann, Hielscher and Schaeben 2010). Those interested on MTEX toolbox can visit the MTEX online tutorials: https://mtex-toolbox.github.io/documentation.html for more details and how to create their own scripts.

Strain measurements were performed on the G5-2 Two Axis Diffractometer "DIANE" of the LLB. The incident wavelength was fixed at 4.7Å and the main αSiO_2 reflection $\{10\bar{1}0\}$ was considered, which corresponds to a scattering $2\theta \approx 90°$. The investigated volumes, as

defined by the instrumental gauge volume, were 5×5×5 mm^3 for the global examinations in the core of the quartzite samples and 3×3×3 mm^3 for local positions inside the sample. Local and global information related to the variations of the magnitude of the lattice spacing as a function of ($\phi\psi$) will be helpful for the assessment and the reliability of the loading conditions. Several $\vec{Q}(\phi\psi)$ orientations with $\phi = 0°$, 30°, 45°, 60° and 90° and $\psi = 0°$, 15°, 22.5°, 30°, 37.5°, 52.5°, 60°, 75° and 90° were measured to ensure a good accuracy of the complete tensor calculation. The specific strain free references $d_0(hkil)$ for each quartzite samples have been determined by the powder method. The powders considered to be completely relaxed of stresses were obtained exactly from the investigated volume of each sample to account all the proper chemical and microstructural irregularities.

4. RESULTS

4.1. Experimental measurement of textures

Figure 5 shows the recalculated {0001} pole figures of the different investigated samples. For each of them, the volume fraction of deformation $\{\bar{1}2\bar{1}0\}<\bar{1}010>$ and recrystallization $\{\bar{1}10\bar{1}\}<\bar{1}\bar{1}20>$ components as well as the texture index are summarized in Table 1. Thereafter, samples are presented from the most deformed state to the most recrystallized one, i.e. samples 131 (deformed), TB and TA (partially recrystallized), 59 and 14 (recrystallized).

The 131 sample exhibits a strong deformation texture. This is confirming the microstructural observations where the 131 sample was sheared along the lineation direction (LD) (Guezou et al. 2001).

The {0001} pole figure of TB sample indicates that both deformation and recrystallization components are present with almost equal fraction (see Table 2). The texture strength index strongly decreases in this sample compared to the deformed 131 sample. The heterogeneous microstructure of the sample collected in Turkey results from the tensile deformation as can be seen from the macroscopic photo in Figure 6. This figure shows the necking of the quartzite sample between the areas where the measurements of TA and TB samples were taken.

The TA, 59 and 14 samples exhibit a typical recrystallization texture as can be clearly seen in their {0001} pole figure (Figure 5) even if a low deformed component is detected for the first sample (Table 1). However, the volume fraction of recrystallization components is higher in TA sample (15.9 %), followed by 59 sample (7.7 %) and then 14 sample (5 %).

Previous microstructural observations demonstrated that 59 and 14 samples were largely affected by primary recrystallization and both samples are nearly free of brittle second phases (Albertini et al. 1991).

4.2. Experimental measurement of residual strains

Figure 7 presents the evolution of ε as a function of $\sin^2 \psi$ at three positions $\phi = 0$, 45 and 90° obtained from $\{10\bar{1}1\}$ reflexion for 131 and 59 samples, respectively. The 131 and 59 samples were presented here to investigate qualitatively the effect of deformation and recrystallization texture on the evolution of residual strains.

As shown in Figure 7a, the evolution of ε for the 131 sample exhibits a non-linear behaviour, or as called a snake-like distribution, at three positions (ϕ = 0, 45 and 90 °), indicating that shear strain components are present due to the deformation nature of the sample. The non-linear behaviour disappeared with decreasing texture strength and changing the texture from deformation to recrystallization as can be observed in sample 59 (Figure 7b). In this case, the evolution of strain is very similar in three positions (ϕ= 0, 45 and 90 °) which may indicate an isotropic behaviour.

Even with the presence of anisotropic and heterogeneous microstructure of the sample 131, all the strain tensor components have been calculated with mean error $\leq 30 \times 10^{-6}$ as presented in Table 2. The strain tensors for the sample 59 and the other samples (TB, TA and 14) are also presented in Table 2. It is must reminded that the strain tensors were calculated with a d_0 value obtained from powder prepared by crushing the considered samples. Consequently, all the quantitative strain values presented in this paper are obtained in the same conditions. Obviously, as it can be seen from Table 2, the samples with low texture strength index, in particular the recrystallized samples (59 and 14), have low strain components values compared to the deformed one, as the 131 sample.

To investigate the effect of size and heterogeneity of diffraction volume on the residual strain values local measurements from back to front of the strongly deformed 131 core sample have been achieved by changing the finite volume of gauge from $5\times5\times5$ mm^3 to $3\times3\times3$ mm^3 (Figure 8).

Moreover, the measurements were performed along the macroscopic sample ND-LD (ϕ = 0°; 0 °< ψ < 90°), ND-TD (ϕ = 90°; 0° < ψ < 90°) and LD-TD (0° < ϕ < 90°; ψ = 90°) planes. The evolution of ε as a function of tilt angle along these planes is shown in Figure 8 for sample 131 and in Figure 9 for the other samples.

The evolution of the strain of the 131 sample is not monotone (Figure 8) with the tilt angle, as expected if the intergranular stresses were absent, thus demonstrating the presence of strain heterogeneities within the diffracting volume.

Figures 8 and 9 show also that the distribution of strain in all samples depends slightly on the sample reference (ND-LD, ND-TD and LD-TD). As can be seen, the distribution of strain along the sample reference plane in small volume gauge (Back and Front measurements) is almost similar by taking into account the error bars. However, qualitatively either global and back/front strain distributions in the sample references own some similarities of their maximum and minimum values versus the tilt angle (especially for the ND-LD plane (black curves), for example) indicating more or less a "large scale" homogeneity as defined for the macro-strains.

The evolution of ε as a function of tilt angle of 59 and 14 samples (Figure 9) are nearly similar along the ND-LD, ND-TD and LD-TD planes mostly due to their weak texture and recrystallized microstructure (Albertini et al. 1991). The TA and TB samples that have both deformed and recrystallized grains present an intermediate behaviour.

The present experimental data, namely the complete strain tensors derived from neutron measurements, provide an opportunity to test it in a numerical texture modelling of quartzite.

4.3. Application to numerical modelling of texture

It has been postulated that the residual strain tensors could have been in part inherited from the total plastic strain supported during the flow of the rock and thus may provide a window into a natural plastic strain tensor responsible of the texture development. If, for example, these elastic strains accommodate the plastic incompatibilities between the matrix and a hard second phase or local cluster of hard grains the compressive strains systematically observed along the stretching direction of the macroscopic deformation would correspond to a back strain, a usual assumption in residual strain analysis (Barrera and Dutta 1993).

Accordingly, the most significant residual strain tensors obtained have been transformed after simplification into plastic strain tensors of which the form and the magnitude of the components could be tested in numerical modelling of the texture of the corresponding sample.

To achieve the transformation, the sign of the main strain components of the matrix have been reversed, owing to the back strain effect and adjusted to keep the sum of ε_{ii} equal to zero. Moreover, all the values closed to the error values ($\leq 30 \times 10^{-6}$) have been set to zero. It

is worth noting that these strain tensors always include significant values for all the ε_{ii} components and at least one shear component. The purpose of the present investigation is to use the residual strain tensor transformed into a plastic one as an experimental parameter in contrast to the earlier simulations of deformation textures, where usually plane strain conditions were used.

Self-consistent models developed for the prediction of the mechanical behaviour of polycrystals are based on treating each grain with its elastic anisotropic properties, or cluster of grains, as local inhomogeneities embedded in an homogeneous equivalent medium having the same overall response as the polycrystal (Wenk et al. 1989, Lebensohn and Tomé 1993, Molinari, Ahzi and Kouddane 1997). Usually, as far as residual strain/stress are concerned, the evolution of intergranular stresses are considered with Elasto-Plastic Self-Consistent (EPSC) formulation (Turner and Tomé 1994, Burnley and Zhang 2008).

In this present work, the development of the elastic component is regarded as a consequence of the whole strain recorded by the polycrystal in a plastic regime. Thus, Visco-Plastic Self Consistent (VPSC) polycrystal model, which is widely used to analyse texture development associated with plastic forming of metals, is relevant and suitable for numerical simulation of geomaterials (Kocks et al. 2000). However, until now such treatments fail to simulate properly the quartzite textures experimentally determined.

The data used for the simulations involve a combination of three plastic modes which have been considered in previous works by Lister and Hobbs (Lister and Hobbs 1980) and later by Wenk et al. (Wenk et al. 1989) as representative of the activity of slip systems at middle to high temperature conditions. The latter conditions are those which have been prevailing during the strain development in the studied quartzite. The slip systems are: basal $\{0001\}\langle 11\bar{2}0\rangle$, prismatic $\{10\bar{1}0\}\langle 11\bar{2}0\rangle$ and pyramidal $\{10\bar{1}1\}\langle 11\bar{2}3\rangle$ and their relative critical resolved shear stress (CRSS) ratios are those used by the authors mentioned above (Wenk et al. 1989). No strain hardening can be reasonably introduced and the coefficient of strain rate sensitivity is set to 3 (correspondent to creep conditions) which is usually used for rocks and minerals. The one site VPSC model has been achieved following a computation by Lebensohn and Tomé (Lebensohn and Tomé 1993). The texture was introduced in the model by a set of 1 000 grains characterized by Euler angles (φ_1, Φ, φ_2). The initial texture was then random or resulting from a first stage of texture simulation. The von Mises equivalent strain ε_e has been implemented by steps of 0.025 until final values of ε_e = 0.5, 1.0 or 2.0.

The innovative point among the input parameters rely on the form of the strain tensor obtained from the experimental residual strain. As an example, the strain tensor of TA sample

has been selected after considering the macroscopic deformation revealed in its field location. This sample undergoes preferentially a tensile behavior with, however, the presence of a σ_{23} strain component as can be seen from Table 2. Hence, this named "tensile" strain tensor of sample TA was transformed into:

$$[\varepsilon] = \begin{bmatrix} 0.8 & 0 & 0 \\ & -1 & 0.3 \\ & & 0.2 \end{bmatrix} \times 10^{-6} \quad (5)$$

The predicted textures presented via {0001} pole figures of TA sample are shown in Figure 10. The experimental {0001} pole figure was also presented for comparison (Figure 10a). The simulation was performed with increasing the strain for ε_e = 1 and 2 as shown in Figures 10b and c, respectively. For the first calculation up to ε_e = 1, the texture was assumed randomly distributed and then the predicted texture was used as input data for the second calculation up to ε_e = 2.

The most remarkable result is the fit of the pole maximum of the TA sample with the deformation direction ensuing the application of the full experimental strain tensor.

From this calculation, it appears on one hand, that a tensile strain leads to a pole centred in the {0001} pole figure and on another hand, that the shear strain component leads to a rotation of this pole around LD.

Then, to simulate the texture of the TB sample, a combination of a "tensile" strain tensor and a "shear" strain tensor was used. This last one was determined in a previous study (Guezou et al. 2001) and was simplified into:

$$[\varepsilon] = \begin{bmatrix} 1 & 0.5 & 0 \\ & -0.8 & 0 \\ & & -0.2 \end{bmatrix} \times 10^{-6} \quad (6)$$

In fact, the experimental strain tensor of TB sample was not applied because its component values are too low to allow a good texture prediction. Hence, the texture prediction of TB sample was performed in two stages. Several simulation combinations were tested but only one is presented in Figure 11. The first stage consists of using the "shear" strain tensor (equation 6) until ε_e = 0.5 by assuming a random texture as input data. The predicted {0001} pole figure of the first stage of the simulation is shown in Figure 11b. Then, the predicted texture was used as input data in the second stage in which the "tensile" strain tensor defined for the TA sample (equation 5) was assumed up to the same total strain (ε_e = 0.5). The predicted texture of the second stage is shown in Figure 11c. The "shear" strain tensor (with a σ_{12} shear component) implies a very large dispersion of <0001> directions (*c*-axis) along ND as observed in the experimental pole figure but does not show any

reinforcements. On the contrary, as already observed, the "tensile" strain tensor leads to a pole centred in the {0001} pole figure with a very low tilt angle because the total strain remains quite small and the shear effect remains low. Consequently, these last simulations do not allow us to predict perfectly the experimental pole figure.

5. Discussion

Usually, the examination of the experimental measurements of residual strain by the $\sin^2\psi$ method allows to test the homogeneity and isotropy of the continuum by plotting ε or d as a function of $\sin^2\psi$. The curves are almost linear with positive or negative slopes if the deformation is tensile or compressive, respectively. However, for highly deformed materials, an oscillation of the ε or d against $\sin^2\psi$ curve is often observed, particularly when the deformation path is complex as frequently observed in natural rock samples. This is confirmed by the evolution of ε as a function of $\sin^2\psi$ for the deformed 131 (snake-like distribution) and recrystallized 59 (linear behaviour) samples as shown in Figure 7. The physical meaning of the non-linear behaviour can be mainly attributed to two factors: 1) the effect of texture on the diffraction elastic constants (Wang et al. 2002), and 2) the microstructural inhomogeneity of the natural rocks. As shown in Figure 5 and Table 1, the 131 sample exhibits a typical deformation texture and consistency texture (I = 10). In addition, the microstructure of sample 131 was characterized by the presence of brittle second phase as shown in Figure 4. In this case, the second brittle phase will definitely cause more local strong elastic strain anisotropy.

In metals, it is generally observed that during the evolution of recrystallization process, grains with higher stored energy and boundaries with lower misorientations angle (θ <15°) are likely to be eliminated, thereby changing the distribution of lattice orientations (texture) and their corresponding misorientations. It is possible to analyse the misorientations based on the orientation distribution function (ODF) which known as the misorientation distribution function (MDF) (Pospiech, Sztwiertnia and Haessner 1986). Figure 12 presents the distribution of the grain boundary misorientation calculated from the ODF of deformed 131 and recrystallized 59 samples. It can be seen that the misorientation distribution is very different between the deformed and recrystallized samples. As expected, the deformed sample shows a large fraction of low angle grain boundaries (misorientation θ <15°) and on the contrary, the recrystallized sample presents a large fraction of high angle grain boundaries (θ >15°) with a high mobility. It is interesting to note that the misorientation distribution of the

deformed 131 sample shows a local peak at 30° which corresponds to grain boundaries with a misorientation of 30° around a <0001> direction. This may be responsible for the formation of the deformation $\{\bar{1}2\bar{1}0\}<\bar{1}010>$ texture, very similar to the formation of basal texture in deformed metals such as magnesium-based alloys (Valle, Pérez-Prado and Ruano 2002).

Table 2 shows that the strain tensor components of the 131 deformed sample are high compared to the 59 and 14 recrystallized samples. The magnitude and distribution of stresses/strains are likely to be dependent on the strength of texture in materials (Vedula et al. 2001, An 1999). The texture index is high in deformed 131 sample (I = 10) followed by TA partially recrystallized sample (I = 2.5) (Table 1) in which both samples present the highest residual strain values (Table 2). In contrast, recrystallized sample such as 59, TB and 14 exhibit a low texture index value (I = 1.8, 1.5 and 1.2, respectively) and as consequence low values of residual strain. Similar observations were reported in cold-rolled and annealed metals like stainless steel (Wang et al. 2002). In this case again intergranular stresses arising from interaction among misoriented neighbour grains during deformation are statistically the contributors to the measured macro or pseudo-macro strains. These findings seem to be in contradiction with what it was found for highly textured ceramic materials, where the residual stresses were found to be lower than those in ceramics with random texture (Vedula et al. 2001, An 1999).

As described above, among the investigated samples, the partially recrystallized TB sample and the completely recrystallized 59 and 14 samples can be considered as mostly relaxed of their residual strains as can be noticed from Table 2. For the other partially recrystallized TA sample, the heterogeneity of strain along the three sample planes (ND-LD, ND-TD and LD-TD) shown in Figure 9b could be attributed to the stronger texture index (Table 1).

Such results may indicate that the heterogeneity of residual strain is more related to the texture sharpness (texture strength index) rather than to the texture type (deformation or recrystallization component).

From Figures 8 and 9, it is also clear that the evaluation of residual strain depends strongly on the experimental condition, like the diffracting volume gauge and the sample reference (ND-LD, ND-TD and LD-TD). This means that for heavily deformed materials, in which the intergranular stress is significant, the reflections do not necessarily provide a reliable measure of the *macro* residual stress as conventionally defined. Subsequently, different second-order stresses could exist, linked to a strong anisotropic plastic deformation

for these plane families, called “pseudo-macroscopic strains” associated with intergranular deformation.

The strain tensor of the sample 131, as obtained at different sampling locations is reported in Table 3. The very different obtained values confirm the presence of large strain heterogeneities within the diffracting volumes, probably due to the interaction of the brittle second phase particles present in the sample with the matrix during the plastic flow. Let us note that in the future, it could be interesting to perform neutron diffraction strain analyses with a bigger gauge volume, for example of the order of $1cm^3$. The obtained values will be probably still more representative of the real deformation history of the rock.

Interestingly, most of the samples share the same feature with a near null or compressive strain within the ND-LD plane, only sample 131 exhibits a tensile strain. In the ND-TD plane, all the samples present a null or a tensile strain. Finally, in the LD-TD plane, a compressive strain is observed for samples TB and TA while a tensile strain is observed for the other ones. The presence of compressive strain within the ND-LD and ND-TD planes corresponds to a response to the plastic stretching along LD.

An interesting perspective could be to analyse the non-linear behaviour such as observed in the strains, notably in the 131 samples, with further extensions of the basic formalism of $\sin^2\psi$ method or try a recent method (Kishan Singh et al. 2014, Guo et al. 2021). Moreover, the electron backscatter diffraction (EBSD) technique, could be very useful to locally investigate the effect of grain orientation on the stored energy and residual strain (Ateba Betanda et al. 2014, Azzeddine et al. 2021).

In section 4.3. the residual strain tensors obtained for TA and TB samples were used as input data for texture simulation using VPSC to predict the deformation texture in quartzite samples. The {0001} simulated pole figures shown in Figures 11 and 12 demonstrated that the proposed approach can be used to improve our understanding of the texture development of geological samples. However, it still remains a qualitative approach, and obviously, the texture cannot be perfectly reproduced especially for the TB sample since the recrystallization is not still taken into account in the VPSC model. In addition, the sharpness and type of the texture depends strongly on the active slip systems. For example, it was found that the domination of <a> slip system produces strong texture while, no texture strengthening was observed when the prismatic <a> slip system is active (Morales et al. 2014). Hence, it is expected that modifying the simulation conditions such as changing the CRSS of active slip systems or using different combinations of slip systems including basal $\{0001\}\langle 11\bar{2}0\rangle$, prismatic $\{10\bar{1}0\}\langle 11\bar{2}0\rangle$ and pyramidal $\{10\bar{1}1\}\langle 11\bar{2}3\rangle$ could improve the texture prediction.

To sum up, and taking into account the limitations described above, the proposed approach allows one to predict the sharp deformation texture that leads to a well-defined elastic strain tensor with significant values of components. Then, in these conditions, it can be used to improve the understanding of the chronology of geological features. In the other cases and in particular when the microstructure is partially or entirely recrystallized it will necessary to improve the present approach including a simulation of the recrystallization textures.

6. CONCLUSION

- The non-linear behavior of ε_{hkil} as a function of $\sin^2 \psi$ distribution usually observed in inhomogeneous weakly anisotropic material is related to a strong plastic deformation combined with the quartz crystal anisotropy.
- The heterogeneity of residual strain is related to the texture sharpness (texture strength index) rather than to the texture type (deformation or recrystallization texture).
- The variations detected by the change of the gauge volume within the deformed sample are attributed to intergranular strains.
- Full residual strain tensors have been determined from neutron measurements and adjusted to fit a plastic tensor injected as an experimental parameter into VPSC model to simulate the natural texture of the corresponding geological samples allowing to have a better knowledge of their strain path.
- To improve this experimental/simulation approach, it could be interesting firstly to analyse samples resulting from simple and unambiguous deformation paths during laboratory deformation tests and secondly to introduce a recrystallization simulation texture.

Acknowledgments

Nicholas J.R. Hunter (Monash University, Australia) is highly acknowledged for the detailed comments and improving the present manuscript.

REFERENCES

Albertini, M. A., T. Baudin, J. C. Guezou & R. Penelle (1991) Texture Study of Naturally Deformed Quartzites From the Betic Cordilleras (Spain). *Textures and Microstructures*, 14**,** 269238.

An, L. (1999) Indentation Fatigue in Random and Textured Alumina Composites. 82**,** 178-182.

Ateba Betanda, Y., A.-L. Helbert, F. Brisset, M.-H. Mathon, T. Waeckerlé & T. Baudin (2014) Measurement of stored energy in Fe–48%Ni alloys strongly cold-rolled using three approaches: Neutron diffraction, Dillamore and KAM approaches. *Materials Science and Engineering: A,* 614**,** 193-198.

Azzeddine, H., T. Baudin, A.-L. Helbert, F. Brisset, Y. Huang, M. Kawasaki, D. Bradai & T. G. Langdon (2021) A stored energy analysis of grains with shear texture orientations in Cu-Ni-Si and Fe-Ni alloys processed by high-pressure torsion. *Journal of Alloys and Compounds,* 864**,** 158142.

Bachmann, F., R. Hielscher & H. Schaeben (2010) Texture Analysis with MTEX – Free and Open Source Software Toolbox. *Solid State Phenomena,* 160**,** 63-68.

Barrera, E. & I. Dutta. 1993. Residual stresses in composites: Measurement, modeling and effects on thermo-mechanical behavior.

Brokmeier, H.-G. 1994. Application of neutron diffraction to measure preferred orientations of geological materials. 327-344.

Burnley, P. C. & D. Zhang (2008) Interpretingin situx-ray diffraction data from high pressure deformation experiments using elastic–plastic self-consistent models: an example using quartz. *Journal of Physics: Condensed Matter,* 20**,** 285201.

Dölle, H. (1979) The influence of multiaxial stress states, stress gradients and elastic anisotropy on the evaluation of (Residual) stresses by X-rays. 12**,** 489-501.

Frischbutter, A., C. Janssen, C. Scheffzük, K. Walther, K. Ullemeyer, J. H. Behrmann, A. N. Nikitin, T. I. Ivankina, H. Kern & B. Leiss (2006) Strain and texture measurements on geological samples using neutron diffraction at IBR-2, Joint Institute for Nuclear Research, Dubna (Russia). *Physics of Particles and Nuclei,* 37**,** S45-S68.

Frischbutter, A., D. Neov, C. Scheffzük, M. Vrána & K. Walther (2000) Lattice strain measurements on sandstones under load using neutron diffraction. *Journal of Structural Geology,* 22**,** 1587-1600.

Gloaguen, D., M. François & R. Guillen (2004) Mesoscopic residual stresses of plastic origin in zirconium: interpretation of X-ray diffraction results. 37**,** 934-940.

Guezou, J.-C., T. Baudin, M. Ceretti, M.-H. Mathon, J.-M. Sprauel & R. Penelle (1999) Étude des déformations élastiques résiduelles dans les quartzites. *Comptes Rendus de l'Académie des Sciences - Series IIA - Earth and Planetary Science*, 328**,** 733-738.

Guezou, J. C., M. Ceretti, T. Baudin, M. H. Mathon & R. Penelle (2001) Elastic Strain Study in Quartzites Using Neutron Diffraction. *Journal of Neutron Research,* 9**,** 357-362.

Guo, J., H. Fu, B. Pan & R. Kang (2021) Recent progress of residual stress measurement methods: A review. *Chinese Journal of Aeronautics,* 34**,** 54-78.

Haworth, F. E. (1937) Energy of Lattice Distortion in Cold Worked Permalloy. *Physical Review,* 52**,** 613-620.

Hunter, N. J. R., V. Luzin & C. J. L. Wilson (2017) Direct measurement of the quartz c-axis using neutron diffraction. *Tectonophysics,* 712-713**,** 464-468.

Hutchings, M. T. & A. D. Krawitz. 1992. *Measurement of Residual and Applied Stress Using Neutron Diffraction*. Springer.

Kishan Singh, C., S. Ilango, S. R. Polaki, S. Dash & A. K. Tyagi (2014) On the evolution of residual stress at different substrate temperatures in sputter-deposited polycrystalline Mo thin films by x-ray diffraction. *Materials Research Express,* 1**,** 036401.

Kocks, U. F., H.-R. Wenk & C. N. Tomé. 2000. *Texture and anisotropy : preferred orientations in polycrystals and their effect on materials properties*. Cambridge: Cambridge University Press.

Lebensohn, R. A. & C. N. Tomé (1993) A self-consistent anisotropic approach for the simulation of plastic deformation and texture development of polycrystals: Application to zirconium alloys. *Acta Metallurgica et Materialia,* 41**,** 2611-2624.

Lister, G. S. & B. E. Hobbs (1980) The simulation of fabric development during plastic deformation and its application to quartzite: the influence of deformation history. *Journal of Structural Geology,* 2**,** 355-370.

Macherauch, E. & K. H. Kloos. 1986. Origin, measurement and evaluation of residual stresses. In *Proceedings of the International Conference on Residual Stresses*, 167–174. Garmisch-Partenkirchen, FRG.

Macherauch, E., P. Müller & Z. Angew (1961) Das Sin^2ψ Verfahren von Rontgenographische Eigenspannungen. *Phys.,* 13**,** 305-312.

Molinari, A., S. Ahzi & R. Kouddane (1997) On the self-consistent modeling of elastic-plastic behavior of polycrystals. *Mechanics of Materials,* 26**,** 43-62.

Morales, L. F. G., G. E. Lloyd & D. Mainprice (2014) Fabric transitions in quartz via viscoplastic self-consistent modeling part I: Axial compression and simple shear under constant strain. *Tectonophysics,* 636**,** 52-69.

Noyan, I. C. & J. B. Cohen. 1987. *Residual Stress*. Springer-Verlag New York.

Pospiech, J., K. Sztwiertnia & F. Haessner (1986) The Misorientation Distribution Function. *Textures and Microstructures,* 6**,** 575690.

Ruud, C. O. (1982) A review of selected non-destructive methods for residual stress measurement. *NDT International,* 15**,** 15-23.

Sander, B. 1950. *Einführung in die Gefügekunde der geologischen Körper*. Springer-Verlag Vienna.

Scheffzük, C., S. Siegesmund & A. Koch (2004) Strain investigations on calcite marbles using neutron time-of-flight diffraction. *Environmental Geology,* 46**,** 468-476.

Scheffzük, C. H., K. Walther & A. Frischbutter (2001) Applied and Residual Strain/stress Measurements on a Dolomite Rock Sample Using Neutron Time-of-flight Diffraction. *Journal of Neutron Research,* 9**,** 187-192.

Schmid, S. 1994. *Textures of geological materials: computer model predictions versus empirical interpretations based on rock deformation experiments and field studies. In: Textures of Geological Materials (H.J. Bunge et al.eds), Deutsche Gesellschaft für Metallkunde, Informationsgesellschaft Verlag, 279-301*.

Skrotzki, W., C. Tränkner, R. Chulist, B. Beausir, S. Suwas & L. S. Tóth (2010) Texture Heterogeneity in ECAP Deformed Copper. *Solid State Phenomena,* 160**,** 47-54.

Suwas, S. & R. K. Ray. 2014. Representation of Texture. In *Crystallographic Texture of Materials*, 11-38. London: Springer London.

Takeshita, T., H.-R. Wenk & R. Lebensohn (1999) Development of preferred orientation and microstructure in sheared quartzite: comparison of natural data and simulated results. *Tectonophysics,* 312**,** 133-155.

Tanaka, K., Y. Akiniwa & M. Hayashi (2002) Neutron Diffraction Measurements of Residual Stresses in Engineering Materials and Components. *Materials Science Research International,* 8**,** 165-174.

Turner, P. A. & C. N. Tomé (1994) A study of residual stresses in Zircaloy-2 with rod texture. *Acta Metallurgica et Materialia,* 42**,** 4143-4153.

Valle, J., M. Pérez-Prado & O. Ruano (2002) The distribution of disorientation angles in a rolled AZ31 Mg alloy. *J Revista De Metalurgia,* 38**,** 353-357.

Vedula, V. R., S. J. Glass, D. M. Saylor, G. S. Rohrer, W. C. Carter, S. A. Langer & E. R. Fuller Jr. (2001) Residual-Stress Predictions in Polycrystalline Alumina. 84**,** 2947-2954.

Walther, K., C. Scheffzük & A. Frischbutter (2000) Neutron time-of-flight diffractometer epsilon for strain measurements: layout and first results. *Physica B: Condensed Matter,* 276-278**,** 130-131.

Wang, Y. D., R. Lin Peng, X. L. Wang & R. L. McGreevy (2002) Grain-orientation-dependent residual stress and the effect of annealing in cold-rolled stainless steel. *Acta Materialia,* 50**,** 1717-1734.

Wenk, H.-R., G. Canova, A. Molinari & U. F. Kocks (1989) Viscoplastic modeling of texture development in quartzite. 94**,** 17895-17906.

Wenk, H.-R., B. C. Chandler, K. Chen, Y. Li, N. Tamura & R. Yu (2020) Residual lattice strain in quartzites as a potential palaeo-piezometer. *Geophysical Journal International,* 222**,** 1363-1378.

Wenk, H.-R., R. Yu, S. Vogel & R. Vasin (2019) Preferred Orientation of Quartz in Metamorphic Rocks from the Bergell Alps. 9**,** 277.

Withers, P. J. & H. K. D. H. Bhadeshia (2001) Residual stress. Part 2 – Nature and origins. *Materials Science and Technology,* 17**,** 366-375.

Zucali, M., D. Chateigner & B. Ouladdiaf (2020) Crystallographic and Seismic Anisotropies of Calcite at Different Depths: A Study Using Quantitative Texture Analysis by Neutron Diffraction. *Minerals* 10**,** 26.

Figure caption

Figure 1: {0001} pole figures calculated with the ideal components related to: (a) deformation $\{\bar{1}2\bar{1}0\}<\bar{1}010>$, and (b) recrystallization $\{\bar{1}10\bar{1}\}<\bar{1}\bar{1}20>$ components. ND is the normal direction to the foliation plan (the rolling plane). LD the direction parallel to the lineation axis.

Figure 2: Schematic illustration of the three orders of residual stresses (σ^{I}, σ^{II} and σ^{III}) in a two-phase (α and β) material (Macherauch and Kloos 1986).

Figure 3: Definition of the sample and laboratory reference directions and the ψ, ϕ angles. ND is the normal direction to the foliation plan (the rolling plane). TD is the transverse direction. L_1, L_2 and L_3 define the laboratory reference. $\vec{Q}(\phi\psi)$ is normal to the diffracting {hkil} planes.

Figure 4: Example of necking of the brittle second phase in sample 131.

Figure 5: Recalculated {0001} pole figures showing the texture of 131, TB, TA, 59 and 14 samples.

Figure 6: Photo of quartzite sample collected from Sivas Basin, Turkey having tensile deformation. The location of TA and TB samples is indicated in the photo.

Figure 7: Evolution of ε as a function of $\sin^2 \psi$ curves showing strain gradient of samples: (a) 131 and (b) 59.

Figure 8: Evolution of ε as a function of tilt angle along the ND-LD ($\phi = 0°$; $0° < \psi < 90°$), ND-TD ($\phi = 90°$; $0° < \psi < 90°$) and LD-TD ($0° < \phi < 90°$; $\psi = 90°$) planes of 131 sample with different diffracting volume labelled (a) global ($5\times5\times5$ mm^3), (b) back and (c) front ($3\times3\times3$ mm^3), respectively. Only two planes were taken into account for the local measurements (b) and (c).

Figure 9: Evolution of ε as a function of tilt angle along the ND-LD ($\phi = 0°$; $0° < \psi < 90°$), ND-TD ($\phi = 90°$; $0° < \psi < 90°$) and LD-TD ($0° < \phi < 90°$; $\psi = 90°$) planes of (a) TB, (b) TA, (c) 59 and (d) 14 samples with diffracting volume of $5\times5\times5$ mm^3, respectively.

Figure 10: VPSC simulations of the deformation texture of TA quartzite sample with the complete strain tensor derived from residual elastic strain tensor measurement. (a) Experimental {0001} pole figure, (b) simulated {0001} pole figure up to $\varepsilon_e = 1$ and (c) simulated {0001} pole figure up to $\varepsilon_e = 2$.

Figure 11: (a) Experimental {0001} pole figure of TB quartzite sample, (b) simulated {0001} pole figure up to $\varepsilon_e = 0.5$ of the first stage and (c) simulated {0001} pole figure up to $\varepsilon_e = 5$ of the second stage.

Figure 12: Misorientation distribution function (MDF) calculated from the ODF of 131 and 59 samples.

Table caption

Table 1: Volume fraction (Fv) of deformation and recrystallization components and texture index of 131, TB, TA, 59 and 14 samples.

Sample	Fv of deformation component (%)	Fv of recrystallization component (%)	Texture index
131	30.5	2.2	10.0
TB	4.6	3.9	1.5
TA	3.3	15.9	2.5
59	0.7	7.7	1.8
14	0.5	5.0	1.2

Table 2. Strain tensors measured by neutron diffraction for the investigated samples. ε_{11} is parallel to the lineation direction (LD), ε_{22} is parallel to the transversal direction (TD) and ε_{33} is parallel to the normal direction (ND).

Sample	$\varepsilon_{11}\times10^{-6}$	$\varepsilon_{22}\times10^{-6}$	$\varepsilon_{33}\times10^{-6}$	$\varepsilon_{12}\times10^{-6}$	$\varepsilon_{13}\times10^{-6}$	$\varepsilon_{23}\times10^{-6}$
131	120±28	61±30	52±16	-18±30	-41±23	-43±9
TB	-38±10	-6±9	12±6	-28±30	-14±9	-7±10
TA	-88±20	110±30	17±20	-7±10	-7±8	-30±20
59	-21±10	36±10	65±6	54±10	-14±8	24±9
14	-23±28	-49±28	54±15	11±25	-1±23	18±22

Table 3. Strain tensors measured by neutron diffraction for the 131 sample.

Sample	$\varepsilon_{11}\times10^{-6}$	$\varepsilon_{22}\times10^{-6}$	$\varepsilon_{33}\times10^{-6}$	$\varepsilon_{12}\times10^{-6}$	$\varepsilon_{13}\times10^{-6}$	$\varepsilon_{23}\times10^{-6}$
131	120±28	61±30	52±16	-18±30	-41±23	-43±9
131 in back	-92±28	-31±30	10±16	-46±30	-22±23	50±9
131 in front	15±28	91±30	-42±16	-46±30	31±23	40±9

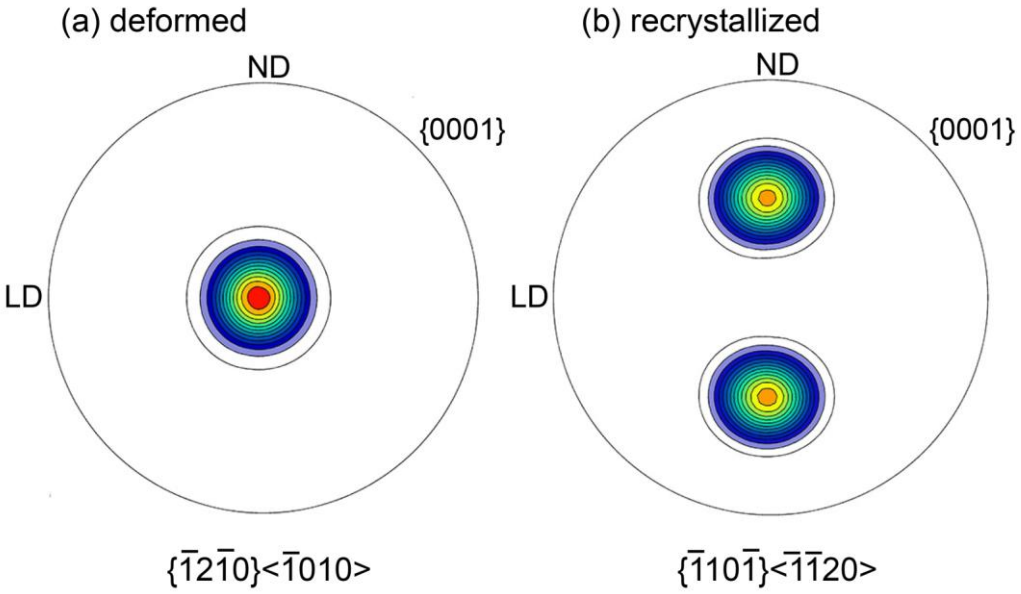

Figure 1

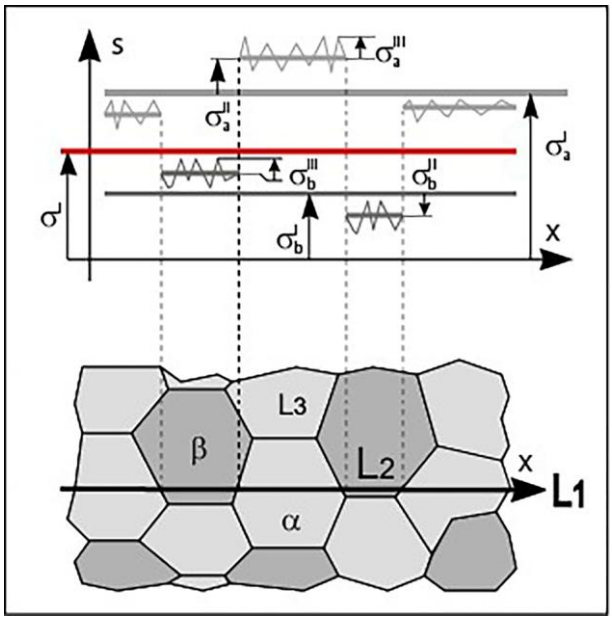

Figure 2

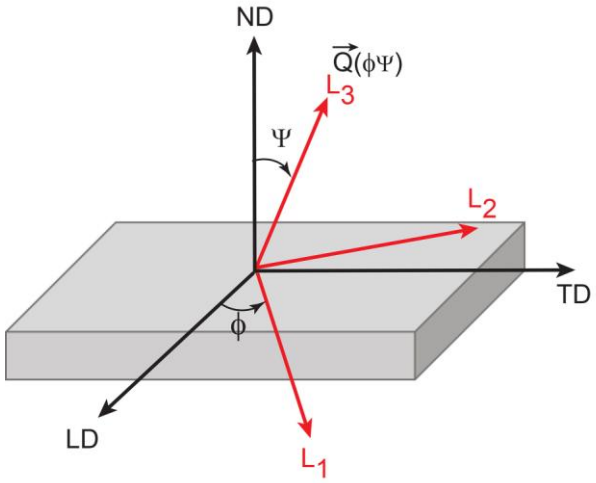

Figure 3

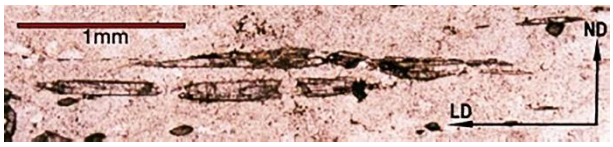

Figure 4

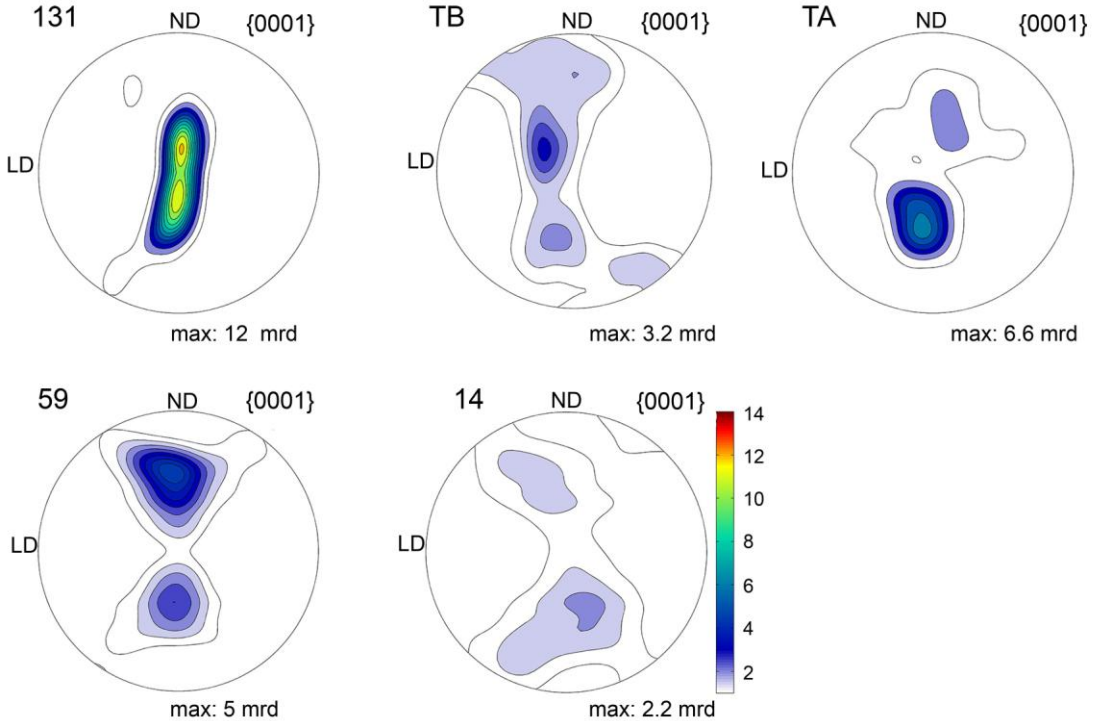

Figure 5

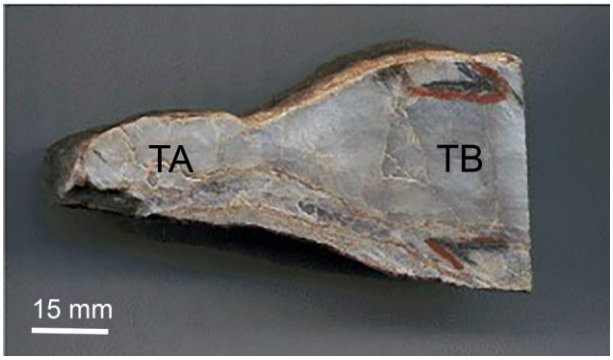

Figure 6

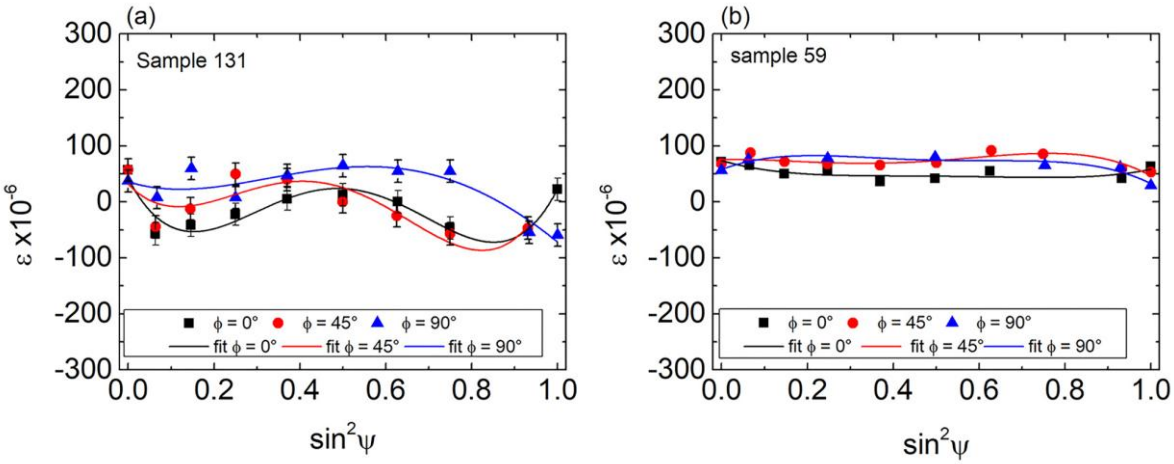

Figure 7

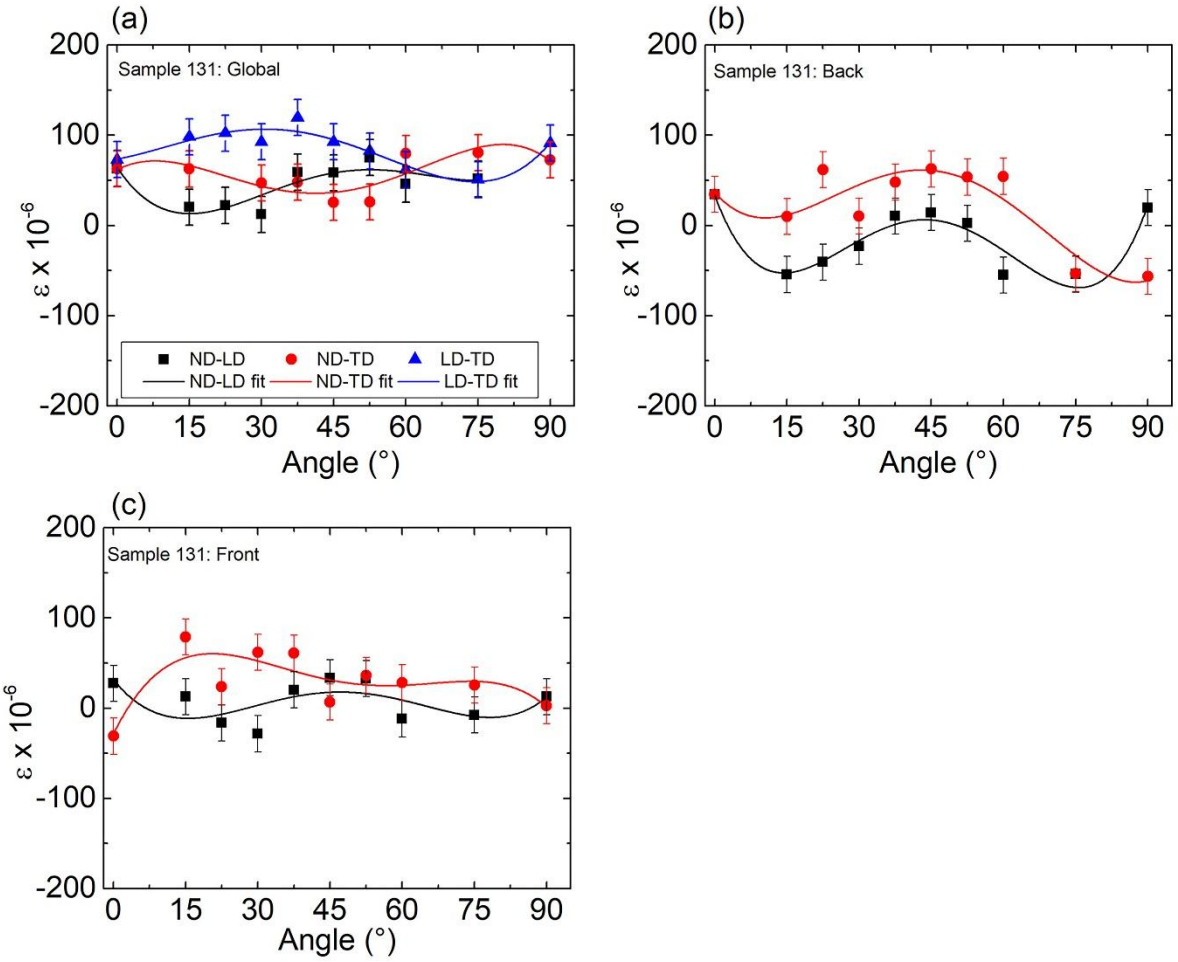
(a)
Sample 131: Global
ND-LD
ND-TD
LD-TD
ND-LD fit
ND-TD fit
LD-TD fit
ε x 10^-6
Angle (°)
(b)
Sample 131: Back
ε x 10^-6
Angle (°)
(c)
Sample 131: Front
ε x 10^-6
Angle (°)

Figure 8

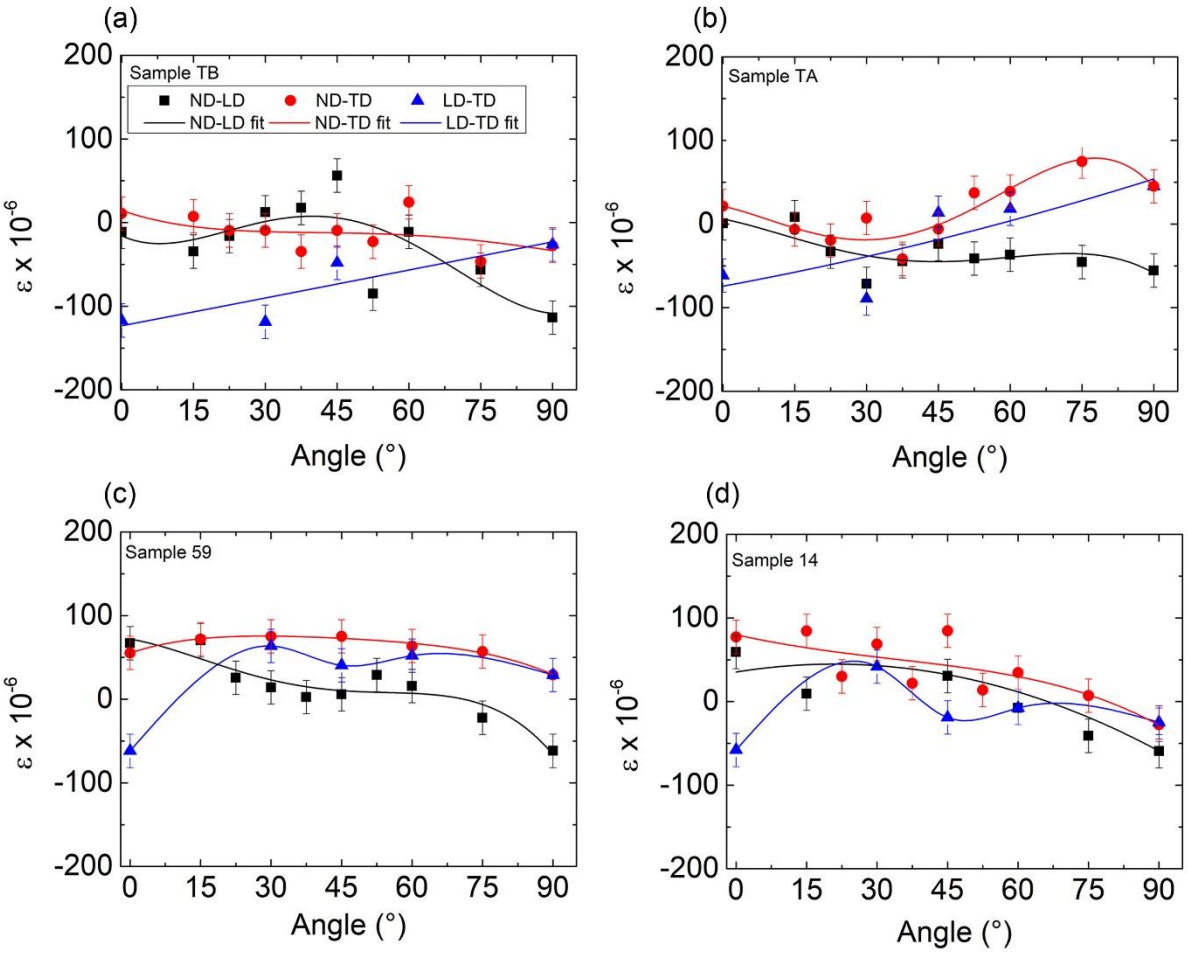

Figure 9

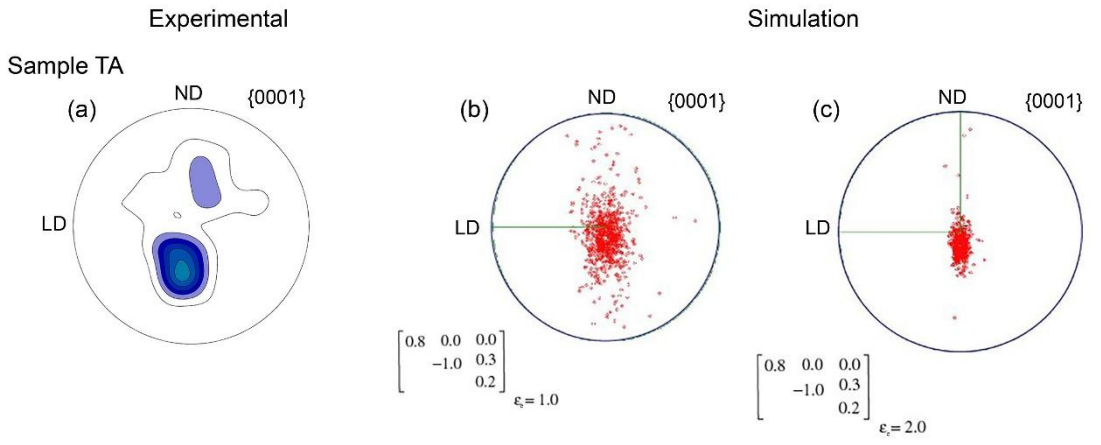

Figure 10

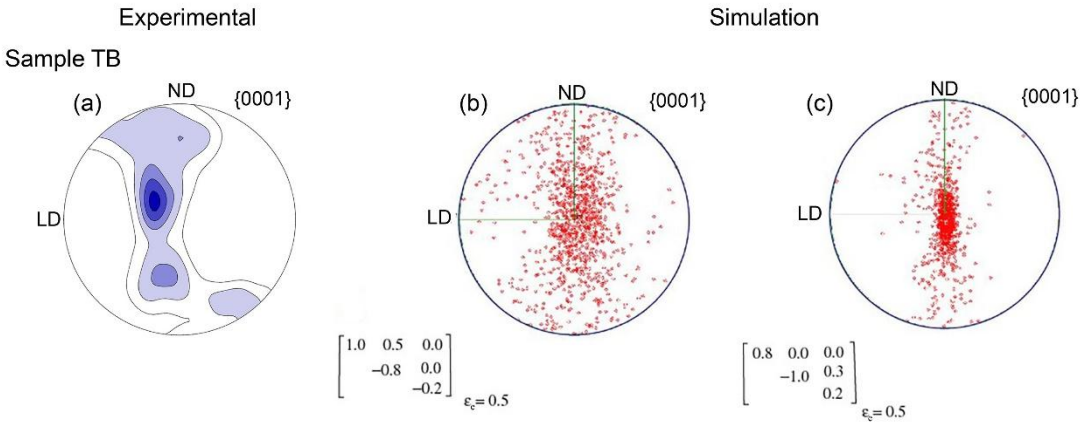

Figure 11

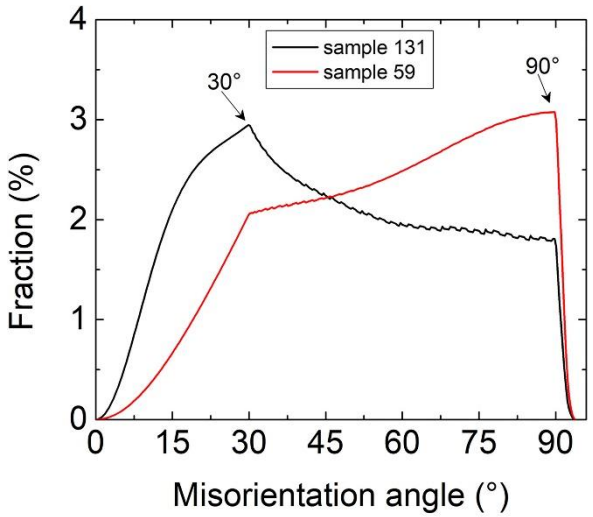

Figure 12